# Gas-Liquid Mass Transfer Characterization in a Thin Shrinking Film at an Atomization Nozzle

Axel Canado, Claude Lemen, Marielle Pages, Frédéric Violleau, N. Dietrich, Gilles Hébrard

# GAS-LIQUID MASS TRANSFER CHARACTERIZATION IN A THIN SHRINKING FILM AT AN ATOMIZATION NOZZLE

Axel CANADO[1,2], Claude LEMEN[2], Marielle PAGES[3], Frédéric VIOLLEAU[1], Nicolas DIETRICH[2], Gilles HEBRARD[2]

[1] *Laboratoire de Chimie Agro-industrielle LCA, Université de Toulouse, INRAE, INP-PURPAN, 31030 Toulouse, France*
[2] *Toulouse Biotechnology Institute TBI, CNRS, INRAE, INSA, Université de Toulouse, 31030 Toulouse, France*
[3] *Physiologie, Pathologie et Génétique Végétales (PPGV) and Plateforme TOAsT, Université de Toulouse, INP-PURPAN, 31030 Toulouse, France*
*Corresponding author: gilles.hebrard@insa-toulouse.fr (G. HÉBRARD)

## Abstract

In this paper, a light absorption method is applied to estimate the thickness of an atomizing liquid film at microscale that exits a spraying nozzle. By using a dioxygen sensitive dye, called resazurin, it is also possible to determine the local profile of dioxygen concentration resulting from the gas-liquid transfer from air into the liquid film. The method relies on the use of the well-known Beer-Lambert law, the linearity of which has been experimentally proved for the optical system and the dye concentration used in this study. From thickness and dye concentration measurements in the liquid film formed at the outlet of the nozzle, a mass transfer analysis is performed, providing a local description of the dioxygen mass transfer (concentration fluxes, etc.) occurring in this film. This optical method, leading to a dual measurement of thickness and mass transfer, is the first to be successfully implemented in this type of thin liquid film in sprays (≈ 30 µm) at microscale and with such high velocities (≈ 8 m/s). The method is non-invasive and does not disturb the flow, in comparison with classical liquid phase measurements where the liquid is collected to be titrated. The values of the mass transfer coefficients, $k_L$, deduced from our analysis for the liquid film ($2.2 \times 10^{-3}$ – $1.2 \times 10^{-2}$ m/s) are consistent with global measurements already obtained, validating our measurement and giving more insight into the mass transfer occurring in this film.

**Keywords:** Film thickness, mass transfer coefficient, concentration measurement, resazurin, spray, , , , light absorption

## 1. Introduction

Spraying processes have been widespread in chemical and industrial applications for years (Ashgriz, 2011). They convert a bulk liquid into dispersions of small droplets in a gaseous environment by giving high velocity to the liquid relative to the surrounding gas. Using kinetic energy, spraying offers a high interfacial area of the dispersed liquid, which leads to many applications in combustion, crop protection, gas treatment and also coating of materials (Lefebvre and Mcdonell, 2017; Lefebvre, 1989).

The process of spray formation can be described as follows: the liquid exits the orifice of the nozzle and forms a thin liquid film a few centimeters long. The liquid film undergoes instabilities due to friction with the gas phase, leading to growing waves in its core. Once the waves reach a critical amplitude, a part of the liquid film breaks into cylindrical ligaments. These ligaments are also torn apart by friction and disrupt into droplets. The liquid in this region has high velocity, growing instabilities in its core, and a window of investigation that is quite small (Lefebvre, 1989; Reitz, 1982). The main parameters used for the characterization of the spray, such as droplet diameters and velocities, length and width of the liquid film, and spray angles, are easily obtained by image acquisition (Dumouchel, 2008; Fansler and Parrish, 2015). The thickness of flowing liquids has been assessed in several ways, using: a conductance method (Kim et al., 2009; Suyari and Lefebvre, 1986), a needle contact method (Rizk and Lefebvre, 1980), and optical methods. Optical methods have the advantage of not disturbing the flow and of bringing together various techniques, including interferometry methods (Koralek et al., 2018) and light absorption methods (Mendez et al., 2016; Zhang et al., 2000).

The large interfacial area and the friction between the dispersed phase and the gas phase, produced by the spray, promote the diffusion of solute between phases. For this reason, spraying processes are very often used in chemical engineering to perform gas depollution since the sprayed liquid absorbs compounds from the gas phase, performing volatile organic compound removal, $CO_2$ capture, $H_2S$ decontamination, etc. The efficiencies of such processes mainly depend on the control of the gas/liquid contact (quality of the atomization, gas flow, etc.) and chemical composition of the phases (Ashgriz, 2011; Hariz et al., 2017; Tatin

et al., 2015).

Mass transfer in spray is commonly well understood when considering liquid droplets exchanging solutes with the gas phase, and many correlations have been proposed to predict the extent of the transfer (Hegely et al., 2017; Lépinasse et al., 2012). Several studies have focused on the liquid film behavior and revealed that the atomizing liquid film that produces the droplets seems to enhance the mass transfer due to its hydrodynamic conditions and interfacial area (Canado et al., 2020; Lin et al., 1977; Simpson and Lynn, 1977; Yeh and Rochelle, 2003). Mass transfer enhancement during the formation stage of droplets or bubbles has also been reported, showing the importance of taking the formation region into consideration for mass transfer applications (Wegener et al., 2009; Xu et al., 2008; Yang et al., 2016).

To quantify the mass transfer enhancement during the formation stage, solute measurements must be made in the region where the droplets are formed. The difficulty of such measurements lies in avoiding any disturbances of the liquid flow in order to measure the composition of the liquid correctly. Although many titration methods exist to quantify a given solute in a liquid, methods giving direct access to the solute quantification without liquid collection, such as Raman scattering spectroscopy, rainbow refractometry, or laser induced fluorescence, are rare or difficult to implement (Lebrun et al., 2021; Lemoine and Castanet, 2013). Liquid collection methods report the global behavior of the mass transfer process, but they lack spatial and time resolution since the liquid collector volume varies with the collection of liquid and the titration is delayed with respect to the moment of collection. Moreover, they involve end effects such as wall collisions, splashes and eddies that can lead to overestimation of the mass transfer. Although various methods are reported in the literature for measuring the temperature of droplets (Brübach et al., 2006; Strizhak et al., 2020; Volkov and Strizhak, 2018; Xue and Zhang, 2018) and their composition (Shao et al., 2012; Srinivasan and Aiken, 1988), no reliable techniques have been proposed for in situ measurement of the mass transfer in the region of the liquid film that produces the droplets.

A recent method for oxygen mass transfer visualization and measurement has been successfully applied to several gas-liquid-solid contactors (Dietrich et al., 2019, 2013; Dietrich and Hebrard, 2018; Kherbeche et

al., 2020, 2013; Mei et al., 2020; Yang et al., 2016). It relies on the light absorption of a dioxygen sensitive dye. In presence of glucose and sodium hydroxide, the dye can be oxidized (e.g., by dissolved dioxygen), and this oxidation leads to a new form of the dye, which absorbs light of a different wavelength. Then, from light absorption, the quantity of oxidized dye, and thence the quantity of dioxygen that has been transferred and has reacted with the dye, can be determined. This method provides solute quantification without disturbing the flow and offers a fun way to visualize the mass transfer.

To the best of our knowledge, there is no optical technique devoted to the dual measurement of thickness and concentration in a sprayed film. Light absorption could be a suitable solution for investigating both hydrodynamics and mass transfer in such a condition. Therefore, the objective of the present study is to implement a light absorption technique for the first dual and simultaneous measurement of mass transfer and film thickness in a free-flowing liquid film produced by a converging fan nozzle before its atomization into droplets.

## 2. Materials

### *2.1. Measurement strategy*

The method presented is based on the use of an oxygen-sensitive dye, rezasurin (CAS n°62758-13-8). This organic chemical compound possesses an interesting property: if subjected to an oxidation/reduction reaction, it produces an intense color when oxidized whereas it is colorless in its reduced form. Note that the oxidation reaction is extremely fast compared to the reduction reaction, which is slow (Yang et al., 2017).

Initially, a solution of resazurin (RZ) in water is dark blue, as shown in Fig.1. In presence of glucose and sodium hydroxide, the resazurin is reduced to its resorufin (RSO) form, which appears pink in solution. This reduction is quite slow and cannot be reversed by oxidation. Further reduction of the resorufin leads to the formation of dihydroresorufin (DHR), which is colorless in solution and is extremely sensitive to oxidation.


Figure 1: Oxidation and reduction reactions for resazurin and its reduced forms.

Any dissolved oxygen in the liquid will react with the DHR to produce RSO and its pink color. As can be seen at the top of the flask of DHR in Fig.1, atmospheric dioxygen dissolves and reacts with DHR to produce a pink layer of RSO. In this way, light absorption through the liquid enables a quantification of RSO, which can be associated with a quantification of the dissolved dioxygen that has transferred and reacted, given that the oxidation stoichiometry is known:

$$2\,DHR + O_2 \rightarrow 2\,RSO + H_2O$$

When spraying a DHR solution in air, $O_2$ from the gas phase is expected to transfer into the solution and to produce pink RSO by reaction. The present method aims to quantify the "pink" produced by the appearance of RSO along the atomizing thin liquid film that leaves a nozzle.

### *2.2. Chemicals*

Table 1 lists the different solutions prepared and sprayed to perform a complete experimental run:

| **Solution name** | **[Rz] (mg/L)** | **[Glucose] (g/L)** | **[NaOH] (g/L)** | **Air bubbling before spraying** |
|---|---|---|---|---|
| Ref | 0 | 10 | 10 | No |

| | | | | |
|---|---|---|---|---|
| Experimental | 200 | 10 | 10 | No |
| Calibration-10 $mgO_2^{eq}/L$ | 200 | 10 | 10 | Yes |
| Calibration-6 $mgO_2^{eq}/L$ | 120 | 6 | 6 | Yes |
| Calibration-3 $mgO_2^{eq}/L$ | 54 | 2.7 | 2.7 | Yes |
| Calibration-2 $mgO_2^{eq}/L$ | 40 | 2 | 2 | Yes |

Table 1. Composition of the solutions prepared and sprayed.

The reference solution "Ref" was composed of 10 g/L of glucose and 10 g/L of sodium hydroxide dissolved in distilled water like all the other solutions but it did not contain any dye. This solution was colorless. The "Experimental solution" was prepared by dissolving 200 mg of RZ, 10 g of NaOH and 10 g of Glucose in a 1 L flask of distilled water. Around one hour later, the solution turned from blue to colorless. At this step, the colorless DHR solution was very reactive with $O_2$. When the Experimental solution was sprayed, atmospheric $O_2$ was expected to transfer into the liquid film and convert the colorless DHR into pink RSO. The "Calibration-10 $mgO_2^{eq}/L$ solution" was prepared in the same way as the Experimental solution except that it was fully oxidized by air bubbling before spraying, to convert all the DHR present in the solution into RSO. In this way, the concentration of RSO in the solution was homogeneous and ensured that the RSO concentration in the liquid film was constant when the calibration solutions were sprayed. The concentration of RSO is expressed in "$O_2^{eq}$". For instance, using the stoichiometry of the oxidation, 120 mg/L of DHR requires the transfer and the reaction of 6 mg/L of dioxygen to fully oxidize the colorless DHR into pink RSO. Several concentrations were prepared from the "Calibration-10$mgO_2^{eq}/L$" by dilution to make standard curves to verify linearity between absorbance, RSO concentration and thickness of the liquid film (Beer-Lambert). The standard curves obtained are presented in the "procedure validation" part.

### 2.3. Image acquisition

To observe any appearance of pink color in the free-flowing liquid film, solutions had to be sprayed and the light crossing the liquid had to be recorded. The experimental set-up shown in Fig.2 was used to obtain images of the free-flowing liquid film atomizing different solutions. First, the solution was contained in a

tank, and a pump (WT3000-1JA, Longer precision pump Co. Ltd, China) sent the liquid to a nozzle that atomized it in front of a CMOS camera (acA9120 – 155um, Basler AG, Germany) equipped with a lens (Nikon AF micro Nikkor f/2.8 lens 60mm). The air feed connected to the tank is used to perform the air bubbling of the calibration solutions to reach complete states of oxidation before spraying. The camera took 1920×800 pixel images with an exposure time of 20 µs at 100 frames per second. Thus, the spatial resolution was 26 µm/pixel. The light source was a LED panel placed behind the liquid sheet, producing white light. A filter located on the LED panel ensured that the light reaching the camera was almost monochromatic, around 550 nm (FWHM=[540nm-575nm]). 500mL beakers were placed under the nozzle to recover the sprayed solution. A fan spray nozzle (AFX-80-02, Nozal, France) with an orifice 1 mm in diameter was used to produce a spray with an 80° angle and droplets around 0.6 mm in diameter. In the range of our operating conditions, the AFX nozzle had the advantage of producing a flat liquid film that could be matched with the focal plane of the CMOS camera.

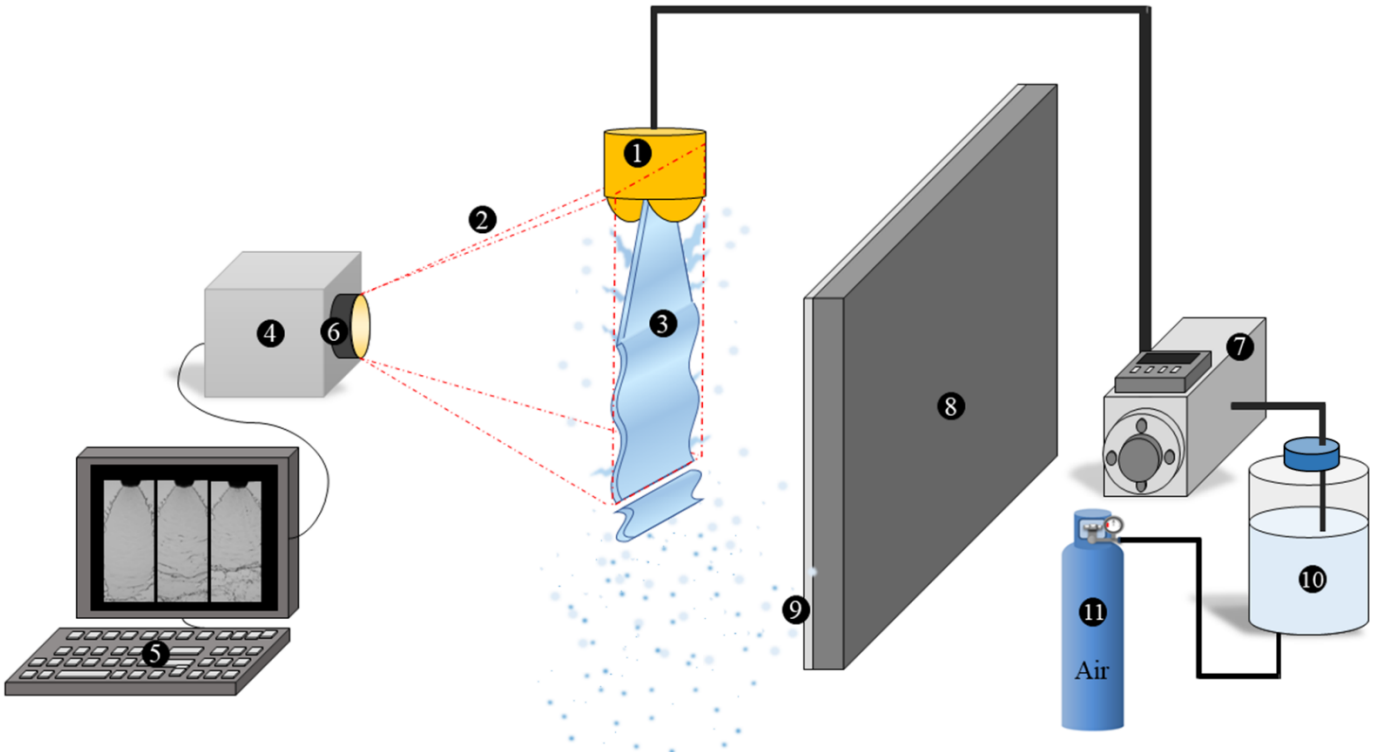


(The nozzle and the liquid film are not to scale compared to the equipment)

Fig.2: Experimental setup for light absorption through the liquid film produced by a nozzle before its atomization in droplets. Nozzle (1), acquisition window (2), liquid film (3), CMOS camera (4), computer (5), lens (6), pump (7), LED panel (8), 550 nm filter (9), 1.5L Bottle (10), air feed (11)

Experiments were repeated 6 times. A complete run of an experiment consisted in spraying all the solutions described in the chemical part and recording the images.

## 3. Methods

### *3.1. Determination of light absorption*

For each solution sprayed, 500 images were recorded with the camera, and 3 different study regions were defined in the liquid film as shown in Fig. 3.

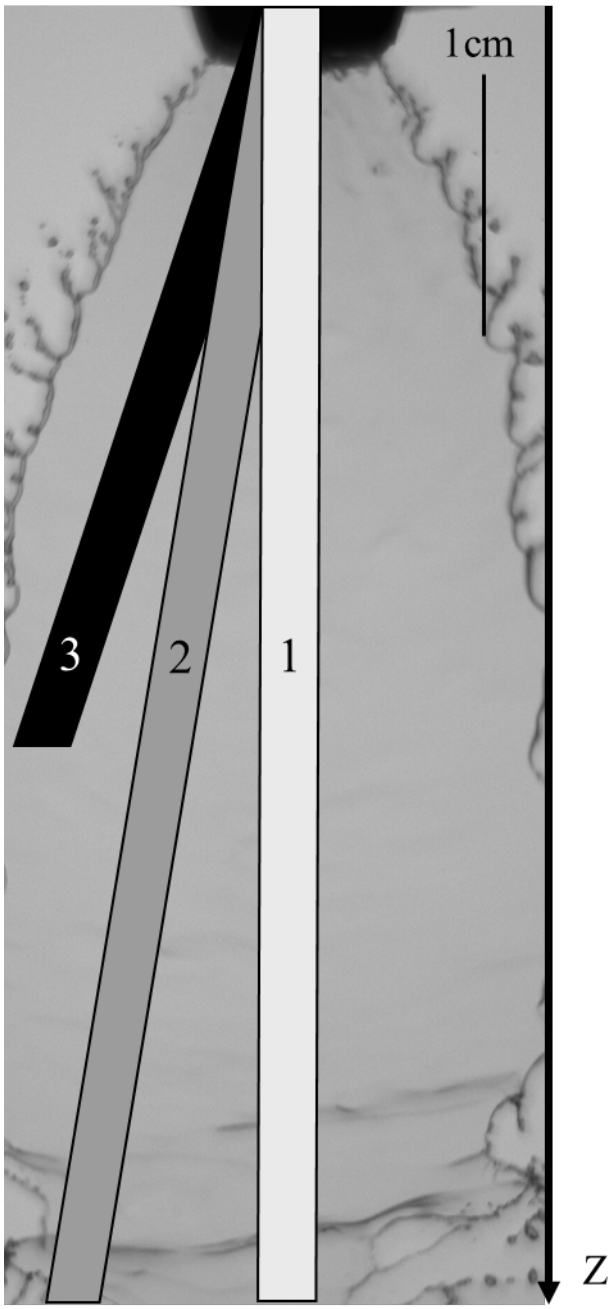


Fig. 3: Image of the liquid film obtained at 22.6 L/h with the experimental setup and the three different

study regions.

Each region has a 100pixel-width and a 1920pixel-length. For each z pixel on the length of the region, the 100 pixels on the width are averaged to obtain a representative value of the intensity in the core of the study region.

Thus, each image $i$ had its own intensity evolution along the film $I_j^i(z) = \sum_{w=1}^{w=100} \frac{I_j^i(z,w)}{100}$ for a given sprayed solution $j$, with w the w$^{th}$.pixel in the width of the region. Then the intensity profile for a sprayed solution was defined as the mean intensity of all the images:

$$I_j(z) = \frac{\sum_{i=1}^{i=500} I_j^i(z)}{500} \quad . \qquad \text{(Eq.1)}$$

A complete run consisted of recording the intensity profile of the reference solution $I_{ref}$, of the calibration solutions $I_{calib10}$, $I_{calib6}$, $I_{calib3}$, $I_{calib2}$ and of the experimental solution $I_{exp}$.

Note that when we refers to "distance in the liquid film", we mean the actual distance travelled on a given streamline, respecting the inclination of region 2 and 3.

### *3.1.1. Beer-Lambert law*

The present method relied on the use of the well-known Beer-Lambert law (Buijs and Maurice, 1969; Swinehart, 1962). The light absorption of a liquid is a function of the thickness of liquid crossed by the light and of the dye concentration for a given wavelength:

$$A_j(z) = \log\left(\frac{I_{ref}(z)}{I_j(z)}\right) = \varepsilon\, \delta(z)\, C_{Rso}(z) \qquad \text{(Eq.2)}$$

With $A_j(z)$ the absorbance (-) of the liquid sheet at the z position for the $j$ condition, $I_{ref}(z)$ the reference intensity at z, $I_j(z)$ the intensity at z for the $j$ solution, $\varepsilon$ the molar attenuation coefficient ($M^{-1}.cm^{-1}$), $\delta(z)$ the liquid thickness crossed by the light at z (cm) and $C_{Rso}(z)$ the dye concentration in the liquid at z (M).

When light from the LED panel crossed the solution, some light rays were refracted at the gas-liquid

interface due to the refractive index difference. This decreased the intensity of the light received by the camera after the liquid sheet. For solutions containing dye, light intensity decrease was expected to be caused by both refraction at the interface and light absorption by the dye. The reference solution served to extract the light intensity decrease due only to the presence of the dye. Its role was the same as that played by the reference solution when measuring the absorbance in a conventional spectrophotometer.

The absorbance was then defined as shown in Eq.2, and one goal of the study was to find the linear relationship between absorbance, thickness, and concentration. If it was verified for our optical system, it would then be possible to access the parameters mentioned above from an absorbance measurement of the liquid film. This verification is presented in the "procedure validation" part.

*3.1.2. Thickness measurement*

Thickness measurements were performed by spraying the "Calibration" solutions that had a homogenous concentration of dye $C_{RSO,j}$. With those solutions, no reaction of DHR with atmospheric $O_2$ was expected during spraying since all the DHR had been consumed by air bubbling beforehand. Considering the Beer-Lambert law, the thickness of a dye liquid crossed by a light beam can be expressed as:

$$\delta_j(z) = \frac{A_{calib,j}(z)}{\varepsilon\, C_{RSO,j}} \qquad \text{(Eq.3)}$$

$A_{calib,j}$ is the absorbance determined with Eq.2 for the RSO concentration of the j solution. The molar attenuation coefficient was determined by making standard curves of diluted calibration solutions with absorbance measurements made in cuvettes using a conventional spectrophotometer (Jasco V-630, Germany). A complete run of an experiment was performed by spraying the 4 Calibration solutions of known concentrations $C_{RSO,j}$ (10, 6, 3 and 2 $mgO_2^{eq}/L$). It was assumed that the concentration of RSO in the thickness of the liquid was homogeneous.

*3.1.3. RSO concentration measurements*

When the Experimental solution was sprayed, pink RSO was expected to appear along the liquid film due to transfer of atmospheric $O_2$ and reaction with the DHR in the liquid.

The RSO concentration appearing in the liquid film was deduced using the Beer-Lambert law:

$$C_{Rso}(z) = \frac{A_{Exp}(z)}{\varepsilon\ \overline{\delta(z)}}$$

(Eq.4)

with $\overline{\delta(z)}$ the average thickness profile obtained by averaging all the thickness profiles determined by Eq.3, and $A_{Exp}$ the absorbance determined with Eq.2 for the Experimental solution.

*3.1.4. Equivalent dioxygen transferred and mass transfer coefficient*

From the stoichiometry of the oxidation reaction, and assuming that enough DHR was present in the solution, it was possible to determine the quantity of dioxygen that had reacted with the DHR to produce the profile of RSO concentration in the liquid film. Then, once the RSO concentration profile was known, the equivalent dioxygen concentration profile that explained the appearance of the RSO was expressed:

$$[O_2]_{eq}(z) = \frac{C_{Rso}(z)}{2} = \frac{A_{DHR,j}(z)}{2\ \varepsilon\ \overline{\delta(z)}}$$

(Eq.5)

Using the equivalent dioxygen concentration profile in the liquid film, the mass transfer coefficient $k_L$ can be determined. Considering an elementary volume of the liquid film, the mass balance between the inlet and outlet of this volume along the z-axis can be written:

$$k_L dS\ ([O_2]^* - [O_2]) = Q([O_2]_{inlet} + d[O_2]) - Q[O_2]_{inlet}$$

(Eq.6)

with dS the area of the interface of the elementary volume in m², $[O_2]^*$ the saturation concentration of dioxygen in the liquid at ambient pressure and temperature in mg/L, $[O_2]$ the actual dioxygen concentration in the elementary volume, Q the liquid flowrate in $m^3/s$, $d[O_2]$ the recorded variation of dioxygen concentration between the inlet and the outlet of the elementary volume, and $k_L$ the liquid side mass transfer coefficient in m/s. It was assumed here that concentration in the liquid film was homogeneous along the width and through the thickness of the elementary volume. The concentration change was assumed to concern the z-direction only.

Then the mass transfer coefficient can be expressed as:

$$k_L = \frac{Q}{dS}\frac{d[O_2]}{([O_2]^* - [O_2])}$$

(Eq.7)

The elementary surface dS was assumed to be

$$dS = 2\,w(z) \times dz$$

(Eq.8)

with $w(z)$ the width between two edges of the liquid film and $dz$ the distance between two pixels on the z-axis.

The width profile along the z-axis, w(z), was determined by averaging the distance between the edges of the liquid film using an edge detection algorithm on 50 images. Note that the surface offered by the two sides of the liquid film ($2\,z \times \delta(z)$) was not considered for the surface calculation as it is very small compared to the regular faces.

The actual concentration of dioxygen was expected to be null in the liquid due to the reaction of the transferred dioxygen with the DHR present in the liquid, and oxygen concentration in air is assumed to be constant. Eq.7 can be simplified to determine a local mass transfer coefficient from the concentration variation $d[O_2]$ observed between two pixels $dz$:

$$k_L = \frac{d[O_2]}{dz}\frac{Q}{2\,w(z)[O_2]^*}$$

(Eq.9)

Integration of Eq.9 allowed a global mass transfer coefficient, able to represent the whole liquid film, to be determined:

$$\overline{k_L} = Q\frac{[O_2]_{outlet} - [O_2]_{inlet}}{2\,\overline{w(z)}\,[O_2]^*\,Z}$$

(Eq.10)

with Z the length of the optical window (cm).

*3.1.5. Dimensionless numbers*

Mass transfer and hydrodynamics are commonly related using correlations that involve the use of

dimensionless numbers such as the Sherwood and Reynolds numbers. The Sherwood number indicates the strength of the mass transfer of a solute compared to its diffusion in the liquid of interest:

$$Sh = \frac{k_L}{D_{O_2/H_2O}} \overline{\delta}$$

(Eq.11)

with $\overline{\delta}$ the mean value of the liquid thickness averaged along the film. The thickness of the liquid was considered as the characteristic length since the small thicknesses of the liquid film could promote the liquid film renewal responsible for enhancing the diffusion of the solute. The Reynolds number describing the nature of the flow was defined as:

$$Re = U \frac{\rho_{H_2O}}{\mu_{H_2O}} \overline{\delta}$$

(Eq.12)

with $\rho_{H_2O}$ and $\mu_{H_2O}$ the density and the dynamic viscosity of the water, respectively, and $U$ the liquid film velocity determined considering the flowrate of liquid passing through the 1 mm orifice of the nozzle:

$$U = \frac{Q}{\frac{\pi \, d_{ori}^2}{4}}$$

(Eq.13)

with $d_{ori}$ the diameter of the orifice of the nozzle.

When writing Eq.9, the actual dioxygen concentration in the liquid was assumed to be null. To verify this statement, the Hatta number was used to compare the rate of reaction and the rate of transfer:

$$Ha = \frac{\sqrt{k \, [RSO] \, D_{O_2/H_2O}}}{k_L}$$

(Eq.14)

with k the reaction rate constant between $O_2$ and the DHR ($L.mol^{-1}.s^{-1}$), [RSO] the concentration of dye (mg/L). It is commonly accepted that the reaction does not accelerate the transfer measured when the Hatta number is smaller than 0.3, as has been determined in several studies for resazurin dye (Yang et al., 2017).

### *3.2 Procedure validation*

### *3.2.1 Optical window*

The first step of the method was to determine whether our optical system was consistent with optical theories such as the Beer-Lambert law. An optical theory that can be easily verified is the Fresnel Equation, which indicates the proportion of the light reflected at the interface of an optical medium. Considering a normal incidence of the light beams through a gas-liquid interface, the Fresnel equation (Träger, 2012) relates the intensity before the crossing of the interface to the intensity received after the reflection:

$$\left(\frac{I_{ref}}{I_0}\right)_{theoretical} = \left(1 - \left(\frac{n_{air} - n_{solution}}{n_{air} + n_{solution}}\right)^2\right)^2 \quad \text{(Eq.15)}$$

With $n_{air}$ the optical index of the air ($n_{air}$= 1) and $n_{solution}$ the optical index of the solution ($n_{solution}$ = 1.33). The latter correspond to the index of water at 20°C around 580nm. Note that this index should be slightly higher due to the presence of glucose in the solution (Weber, 2018).

By recording the background intensity $I_0$ received at the camera when no liquid was sprayed and comparing it with the $I_{ref}$, for the vertical study region (region 1), it was possible to plot the fraction of light intensity lost by the successive crossing of two gas-liquid interfaces (Fig.4A).

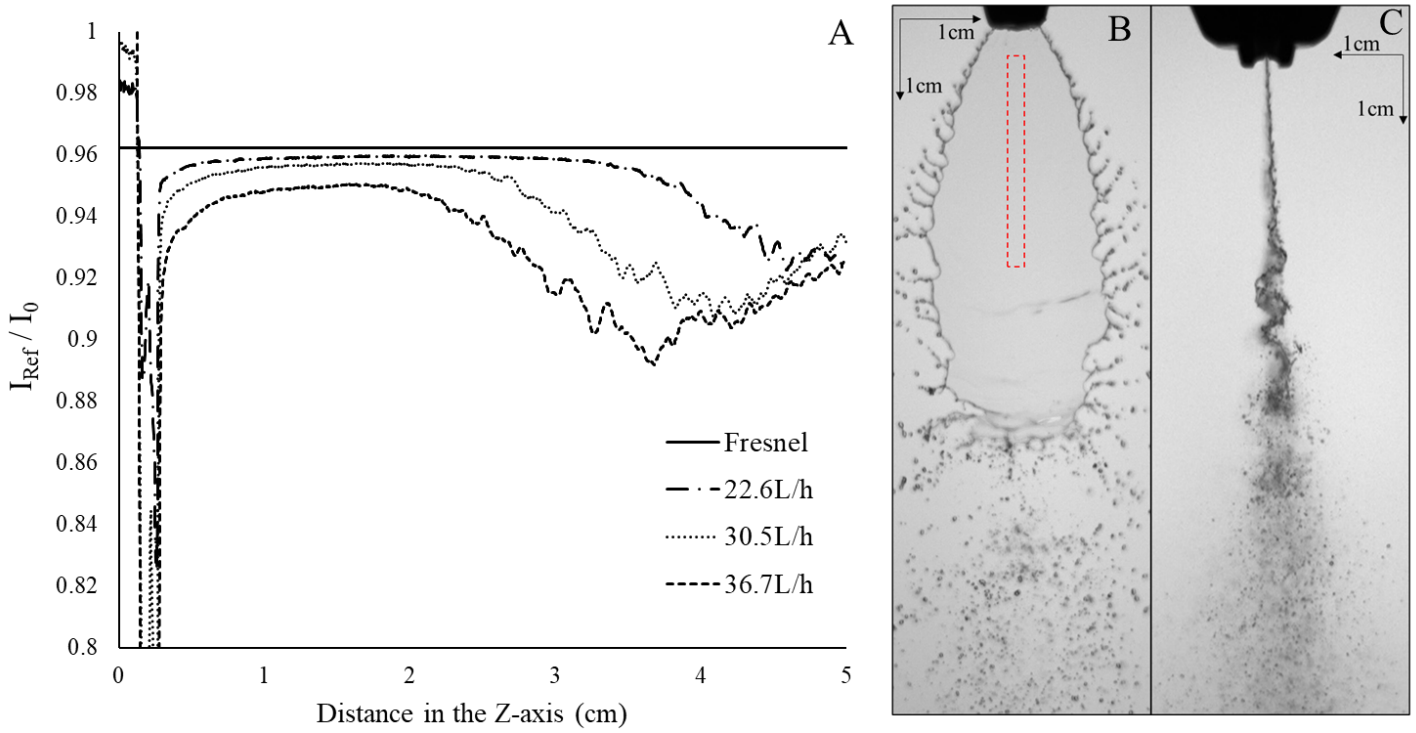


Fig.4: Ratio between the background intensity, $I_0$, and the intensity $I_{ref}$ recorded for the reference solutions

sprayed at different flowrates along the liquid film (A). Images with a larger acquisition window to fully observe the liquid film from the front view (B) and side view (C). The red rectangle represents the largest optical window obtained for the 22.6L/h flowrate.

Note that the strong variation obtained for the experimental curves in Fig.4a between z = 0 cm and z = 0.3 cm corresponds to the part of the image where the nozzle was located. As shown in Fig.4B and C, the light did not cross the nozzle, so this area appeared black with low values of intensities. The ratio between the two intensities varied considerably due to the noise of the camera in this region and the closeness of those low values.

Moreover, in Fig.4A, the second part of the plot, from z=3 cm, also exhibited high discrepancies with Eq.15. This was due to the increase of the amplitude of instabilities in the liquid film as shown in Fig.4C. In this side view, it was possible to observe the increase of the amplitude of waves in the direction of the flow. As can be seen in Fig.4B, dark folds appeared in the liquid, which caused a reduction of the intensity received at the camera.

The instabilities then led to the breakup of the liquid film, and this breakup seemed to be described with the decrease of the second part of the curves. This decrease occurred closer to the nozzle for high flowrates, meaning that the liquid film produced at high flowrate was shorter. However, except at the beginning and the end of the region of study, the experimental curves were in good agreement with Eq.15 and a normal incidence of the light through the liquid film could thus be assumed. This hypothesis was essential for the use of the Beer-Lambert law.

It then seemed necessary to consider an optical window in the images where optical theories were applicable. For the present study, the optical window was defined as the part of the images where the difference between the measured and theoretical $I_{ref}/I_0$ was lower than 1% for the 22.6L/h and the 30.5L/h flowrate. The resulting optical window ranged from 0.3 cm to 2.9 cm in the liquid film for the 22.6 L/h flowrate, and from 0.35cm to 2.5cm for the 30.5L/h. The higher flowrate, 36.7L/h, showed greater differences with the Fresnel theory, the optical window was then defined for a difference of 2% with the theory, leading in a optical window of [0.5cm – 2.0cm].For this reason, the following curves in the study did not start at zero

when describing an evolution inside the liquid film.

*3.2.2 Absorbances & Beer-Lambert verification*

Once the optical window had been determined for each flowrate tested, the absorbance profiles along the z-axis in the liquid film could be determined according to Eq.1 and Eq.2. For a flowrate of 22.6 L/h, the absorbances of the RSO solutions sprayed for a single run along region 1 have been plotted in Fig.5:

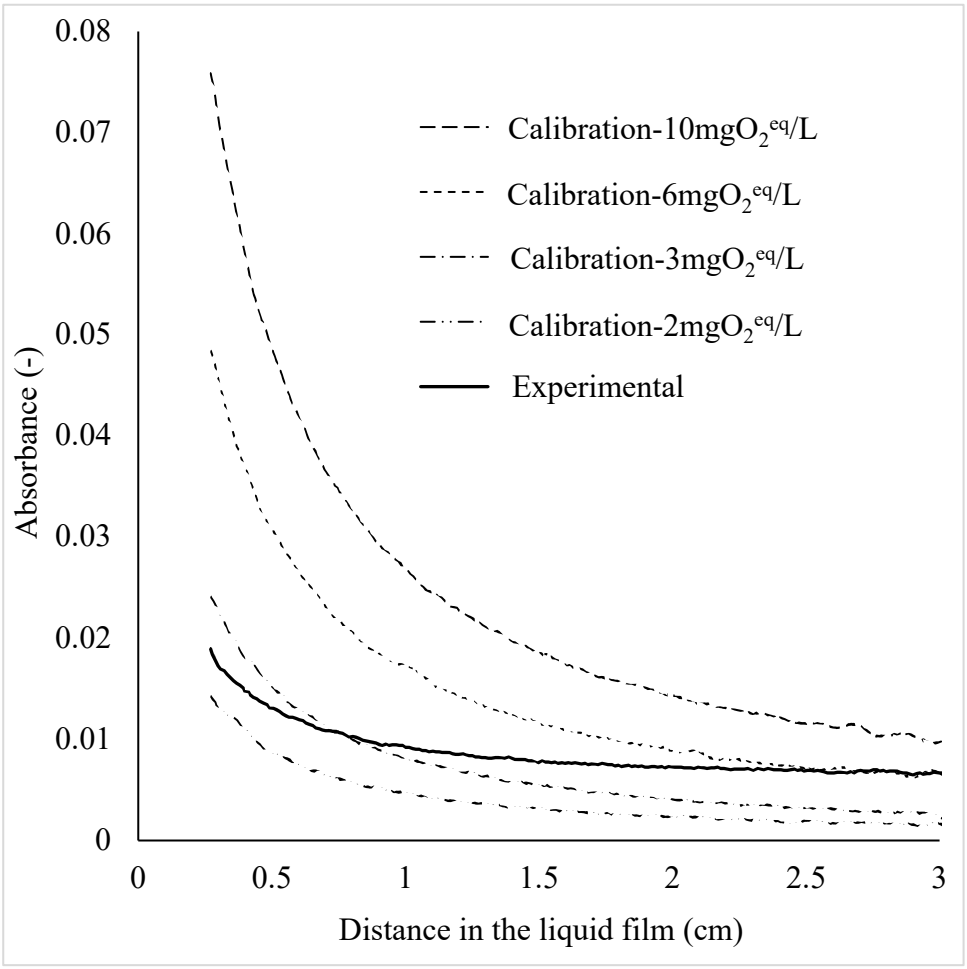


Fig.5: Absorbance profiles along the optical window for different RSO solutions sprayed with constant concentration (calibration solutions) and for DHR solution (experimental) at 22.6L/h.

The Calibration-6 $mgO_2^{eq}/L$ solution containing 120 mg/L of RSO had an absorbance profile higher than the 3 $mgO_2^{eq}/L$ solutions at 54 mg/L. The latter was also higher than the Calibration-2$mgO_2^{eq}/L$ solution with its 40 mgRSO/L, so, for increasing concentrations of dye, the absorbance also increased, consistently with the Beer-Lambert law.

Absorbance profiles of the RSO solutions exhibited a common behavior: the absorbance decreased along

337 the liquid film. According to Eq.2, for a constant concentration of RSO, the only parameter acting on the
338 absorbance was the thickness of the liquid. Thus, the absorbance decrease observed in Fig.5 might be due
339 to a diminution of the thickness of the liquid film along the z-axis. This statement seems justified since
340 volume conservation of a bulk liquid implies that the thickness of the film decreases if its width increases,
341 as seen in Fig.4B.
342 Thus, before a quantitative study in terms of thickness or concentration variation could be performed using
343 the absorbance measurements, the Beer-Lambert law had to be demonstrated for the optical system.
344 *3.2.3 Beer-Lambert verification & RSO spectra*
345 To verify the linearity of the Beer-Lambert law, it was necessary to associate the absorbance measurement
346 with known values of concentration and thickness. While concentrations were easily determined from the
347 mass and volume used for the preparation of the RSO solutions, the thickness of liquid crossed by the light
348 was unknown.
349 For a given flowrate, it was assumed that the nozzle produced a film with a given thickness profile.
350 Instabilities in the film induced the appearance of wavy motions in it and the waves were responsible for
351 local loss of intensity due to oscillations around the focal plane of the lens. They were also the origin of
352 deformations of the interface that perturbed the normal incidence of the light on the film. The spatial
353 occurrence of such instabilities was different from one image to another, so 500 images were averaged to
354 record a maximum of images without the occurrence of waves.
355 Considering the hypothesis put forward above, Fig.6 shows the absorbance measured at a given position
356 plotted against the concentration in RSO of the different solutions sprayed. For a position located 0.52 cm
357 from the border of the image (square in the photo of Fig.6), the evolution of the absorbance measured for
358 the 2, 3 and 6 mg/$LO_2^{eq}$ solutions was linear. This linear correlation between absorbance and concentration
359 was also found for other positions in the liquid sheet, as shown for each slope in Fig.6. The observed
360 linearities validated the fact that the Beer-Lambert law could be used for our optical system. Note that the
361 10mgO2eq/L solution did not respect the linear correlation, probably because of its high concentration in
362 resazurin, since the Beer-Lambert law is available for infinite dilution and without interactions between
363 solutes. For the remaining part of the study, the 10mgO2eq/L solution was not considered.

According to Eq.2, the slope of the curves was the term $\varepsilon \times \delta(z)$. The slopes decreased with the distance into the film. Because $\varepsilon$ is a constant property of the dye, the slope reduction can be explained by the decrease in thickness along the film. Thus, it is possible to conclude that the liquid film leaving the nozzle became thinner as it traveled further from the nozzle.

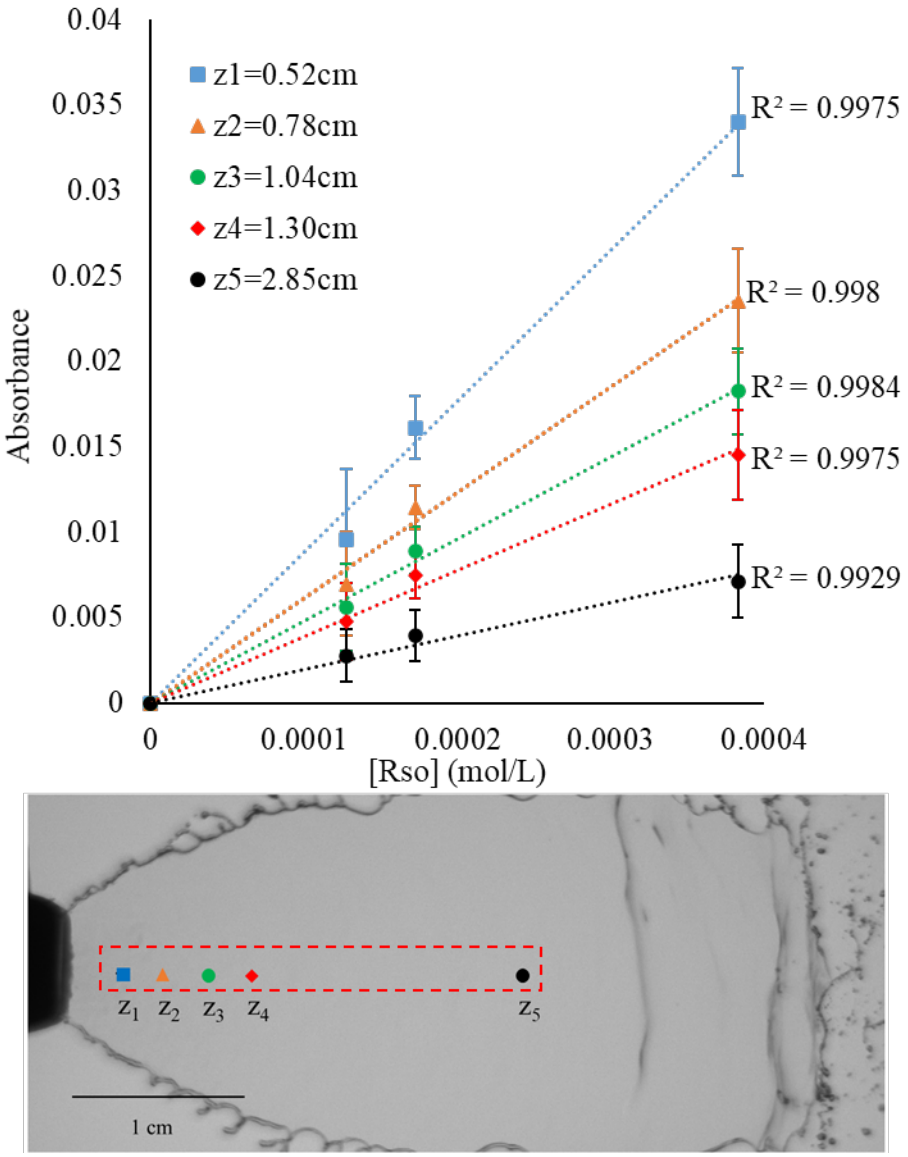


Fig.6: Absorbance of the sprayed RSO solutions versus their concentration for different positions in the liquid film for the 22.6 L/h flowrate in region 1 (top). The positions are indicated on the image of the liquid film with symbols and the red rectangle represents the optical window for the 22.6L/h flowrate (bottom).

The linearity between absorbance and dye concentration being proven, Eq.2 should be valid for making a quantitative analysis of the thickness profile of the film using Eq.3. This implies the determination of $\varepsilon$. The spectra in Fig.7 were obtained with a conventional spectrophotometer (Jasco V-630, Germany):

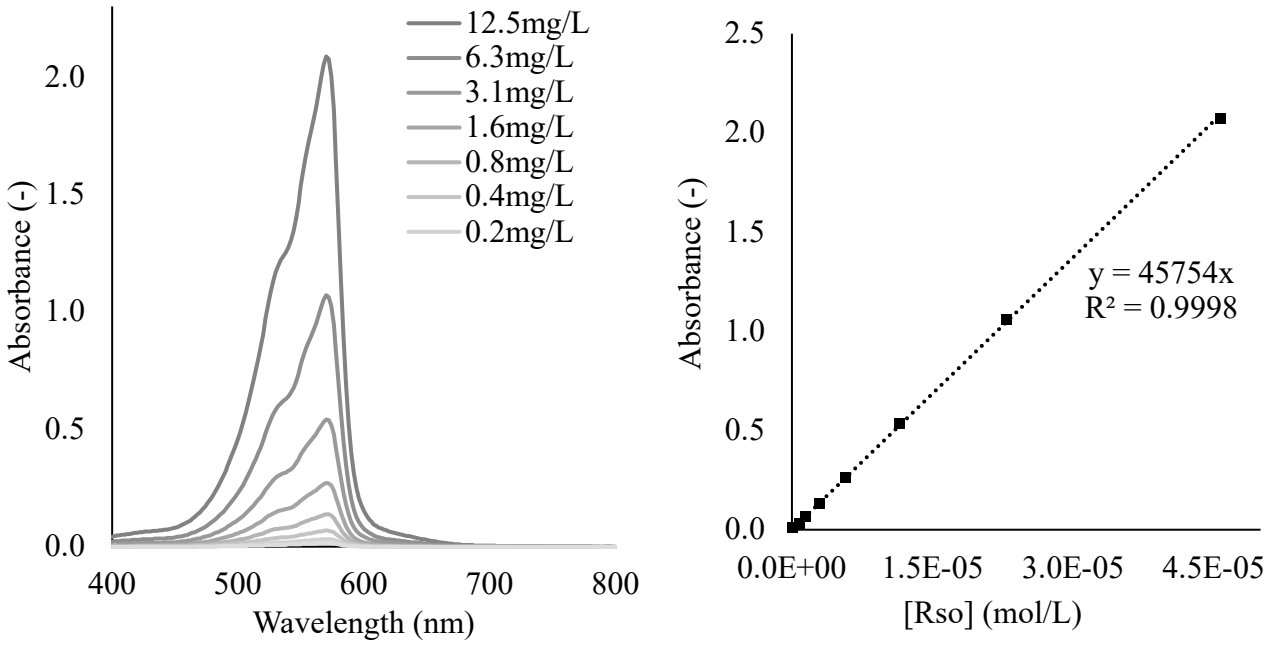


Fig.7: Resorufin spectra in the visible range using a spectrophotometer (left) and the corresponding calibration curve at 572 nm (right).

The resorufin spectra presented in Fig.7 show a maximum absorbance at 572 nm. This was the reason why the 550 nm filter was set up in front of the camera. It ensured that the camera received light that was likely to be absorbed by the RSO. By measuring the absorbance of several diluted solutions at 572 nm, the molar attenuation coefficient was determined to be around 45754 $M^{-1}.cm^{-1}$ as shown in Fig.7. The maximum wavelength and the attenuation coefficient found are consistent with those in the literature (Maeda et al., 2000).

Finally, for the optical setup presented, a normal incidence through the liquid film can be assumed in a defined optical window. This consideration allowed calibration curves to be plotted for the absorbance of sprayed solutions of known concentration. The linearity observed between absorbance and concentration at different places in the liquid film validated the possibility of using the Beer-Lambert law for quantitative

391 analysis of liquid thickness and concentration.

392 ## 4. Results

393 ### *4.1 Hydrodynamic study*

394 *4.1.1 Qualitative observation*

395 Successive images of the liquid film acquired for different flowrates are represented on Fig.8. It was
396 observed that, for increasing flowrates, the angle of the liquid film (initially around 80°) became wider,
397 increasing the width of the liquid film.

398 This seems logical since the increase of the flowrate results in high inertial forces in the liquid (velocity
399 augment), but the surface tensions of the liquid remain constant as an intrinsic property of the fluid. The
400 surface tensions forces maintain the liquid as a continuous volume, but inertial forces, in addition with
401 friction, are in opposition of this phenomenon. The ratio between inertial force and surface tension increases
402 with the flowrate, then allowing the liquid to be more stretched, leading to width increase of the liquid film,
403 and growing instabilities.

404 The presence of folds in the liquid film was thus more frequent for the 30.5 and 36.7 L/h flowrates. As
405 shown in Fig.4A, the breakup of the film seemed to occur closer to the nozzle for those flowrates.

406

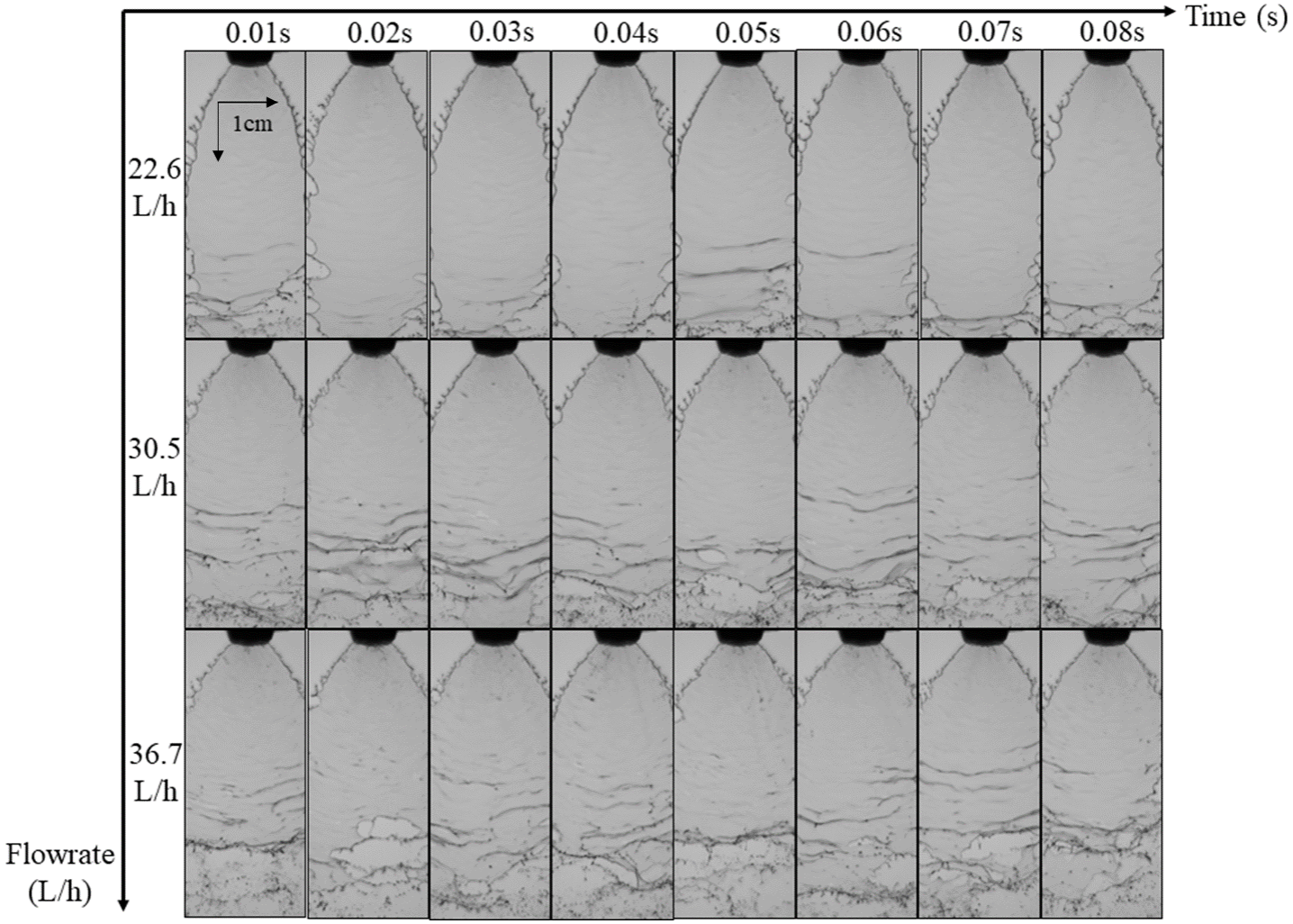


Fig.8: Images of the liquid film at different times for several flowrates.

Although instabilities were present at the bottom of the images for the 3 flowrates, the core of the liquid film seemed quite stable over time in its upper part since no patterns of waves were identifiable there from one image to another.

In all cases, the width of the film increased in the flow direction, until breakup occurred. This is consistent with the hypothesis of the thickness decrease along the z-axis as assumed in the procedure validation section. To respect volume conservation, it seems inevitable that an increase of the width of the liquid film should produce a diminution of the thickness. This qualitative observation can be quantified by image analysis.

*4.1.2 Width profile*

By using an edge detection algorithm to track the edges of the liquid film on 50 pictures with larger field of vision, the distance between the borders of the film can be determined and plotted along the flow direction as shown in Fig.9. The edge detection algorithm was not dependent of the optical windows defined

for the normal incidence of the light, then the measurement starts from the exit of the nozzle, directly when the film is formed. Measurements are shown until the maximum width obtained, because after that the algorithm fails to detect edges due to the presence of folds and breakup of the film.

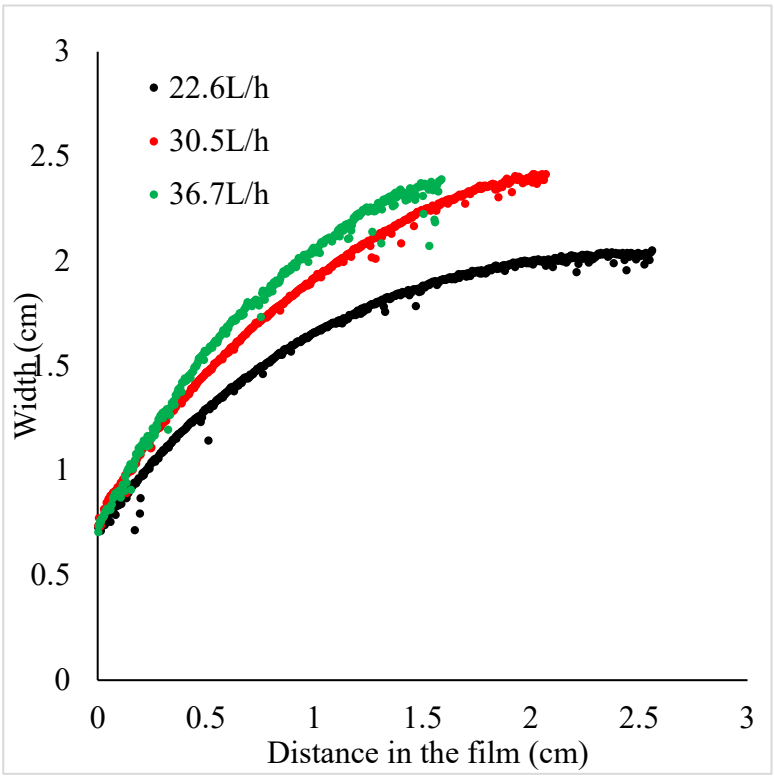


Fig.9: Evolution of the liquid film width with the distance for 3 different flowrates.

This image analysis confirmed that the width of the film increased in the flow direction. The assumption that the breakup occurred closer to the nozzle for increasing flowrates was also confirmed. For increasing flowrates, the width profiles increased more rapidly but the breakup occurred earlier. For instance, with the 30.5 L/h flowrate, the width reached a maximum of 2.4 cm after an evolution of 2.5 cm along the film but, for the flowrate of 36.7 L/h, the maximum width was reached after 2 cm in the film and was equal to 2.2 cm. It could have been expected that the maximum width for the 36.7 L/h flowrate would be higher than that for 30.5 L/h but the breakup occurred before the width at 36.7 L/h exceeded that at 30.5 L/h. In all cases, the width of the film expanded in the flow direction.

The different width profiles obtained in Fig.9 were integrated, from 0cm to their respective maximum width, along the z-axis to evaluate the surface area of the liquid film produced for each flowrate, as proposed with Eq.8. The area obtained for the 22.6 L/h flowrate was 8.51 x $10^{-4}$ m² whereas, for the 30.5 L/h flowrate, the liquid film surface area was 7.61 x $10^{-4}$ m². An area of 5.63 x $10^{-4}$ m² was obtained with the higher flowrate of 36.7 L/h. The total liquid film surface as defined in Eq.8 becomes lower for increasing flowrates as

shown with the calculated values. Although higher widths are reached with higher flowrates, this surface reduction probably results from an earlier breakup of the film due to the presence of more instabilities motions in the liquid film for the high flowrates.

*4.1.3 Thickness profile*

From the different values of the RSO concentration and the molar attenuation coefficient (454754 $M^{-1}.cm^{-1}$), the thickness profiles along the z-axis were determined using Eq.3. The profiles are plotted in Fig.10:

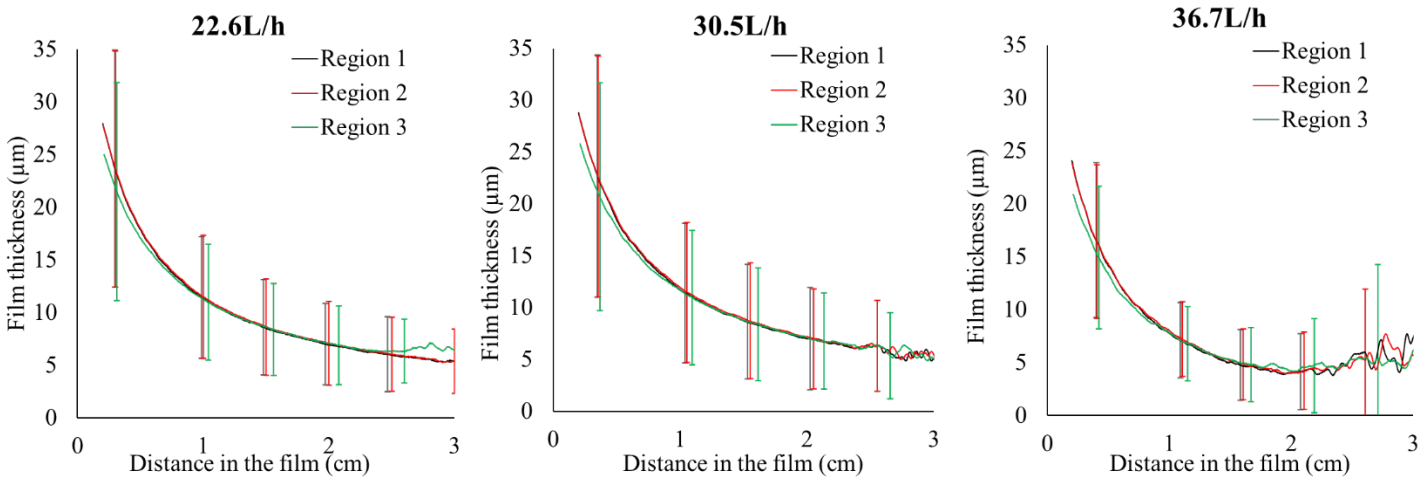


Fig.10: Thickness profiles along the liquid film for different flowrates and regions of study. Errors bars are the standard deviation of the 18 (6×3) thickness profiles acquisitions (3 calibrations solutions per run). For clarity, they are represented only for some points of the profile.

As assumed previously, the liquid film thickness decreased with increasing distance from the nozzle. From around 30 µm at the outlet of the nozzle, the thickness of the liquid film reached values close to 5 µm after a distance of a few centimeters. The thickness profiles of the 3 different flowrates exhibited the same evolution. Note that the thickness profile for the 36.7 L/h seemed lower than for 22.6 and 30.5 L/h. Although the width profiles were different for the 3 flowrates, the thickness profiles were quite similar for the three. Note that we observed a surface reduction of the liquid film when increasing flowrates from the integration of the width profiles, but the thickness profiles seemed not affected by the flowrate. Then, it was possible to state that the volume of the liquid film produced by the nozzle decrease with increasing flowrates.

For each flowrate, the thickness profiles did not depend on the region of study. Region 1, which represented

459 the vertical core of the liquid film, exhibited the same thickness profile as region 3. The latter described a
460 streamline between the core and the edges of the liquid film. Thus, it seemed that the liquid film offered a
461 relatively homogeneous thickness evolution. Note that the "distance in the film" refers to the actual distance
462 traveled on a given streamline, respecting the inclination of each region.

463 ***4.2 Concentration measurements***

464 The goal of the concentration measurement was to quantify the transfer of atmospheric dioxygen to the
465 liquid film by observing the absorbance variation of the liquid film due to the sensitive dye. Once the
466 contribution of the thickness evolution to the absorbance variation in the liquid film had been assessed, the
467 appearance of RSO when spraying a DHR solution could be determined using Eq.4. The absorbance
468 $A_{Exp}$ and the absorbances of the fully oxidized solutions $A_{calib}$ are plotted in Fig.5.
469 The absorbance change along the liquid film for the experiment with DHR solution was produced by both
470 the oxidation of DHR into RSO and by the thickness variation. The absorbance evolution for the other
471 solutions was due only to thickness variation since the concentration of RSO was set constant by bubbling
472 before spraying. Thus, it was possible to see that the Experimental profile did not follow the same trend as
473 the other solutions because of the DHR oxidation and its corresponding change in concentration due to the
474 mass transfer phenomenon. The DHR curve crossed the 3 mg/L-$O_2^{eq}$ and the 6mg/L-$O_2^{eq}$ curves, denoting
475 the increase in RSO concentration in the film.
476 From the absorbance profile of the DHR solution and from the knowledge of the mean film thickness profile,
477 the equivalent dioxygen concentration that would have been present in the film is plotted in Fig.11(A, B,
478 C) using Eq.5. Note that no dioxygen was present in the liquid since the reaction of $O_2$ with DHR consumed
479 any molecule of $O_2$ that dissolved from the air to the liquid. In fact, production of an RSO molecule meant
480 that a dioxygen molecule from the gas had transferred to the liquid and then reacted with a molecule of
481 DHR. The equivalent dioxygen concentration on the y-axis represents the accumulation of dioxygen that
482 would theoretically occur if no reaction took place in the liquid.

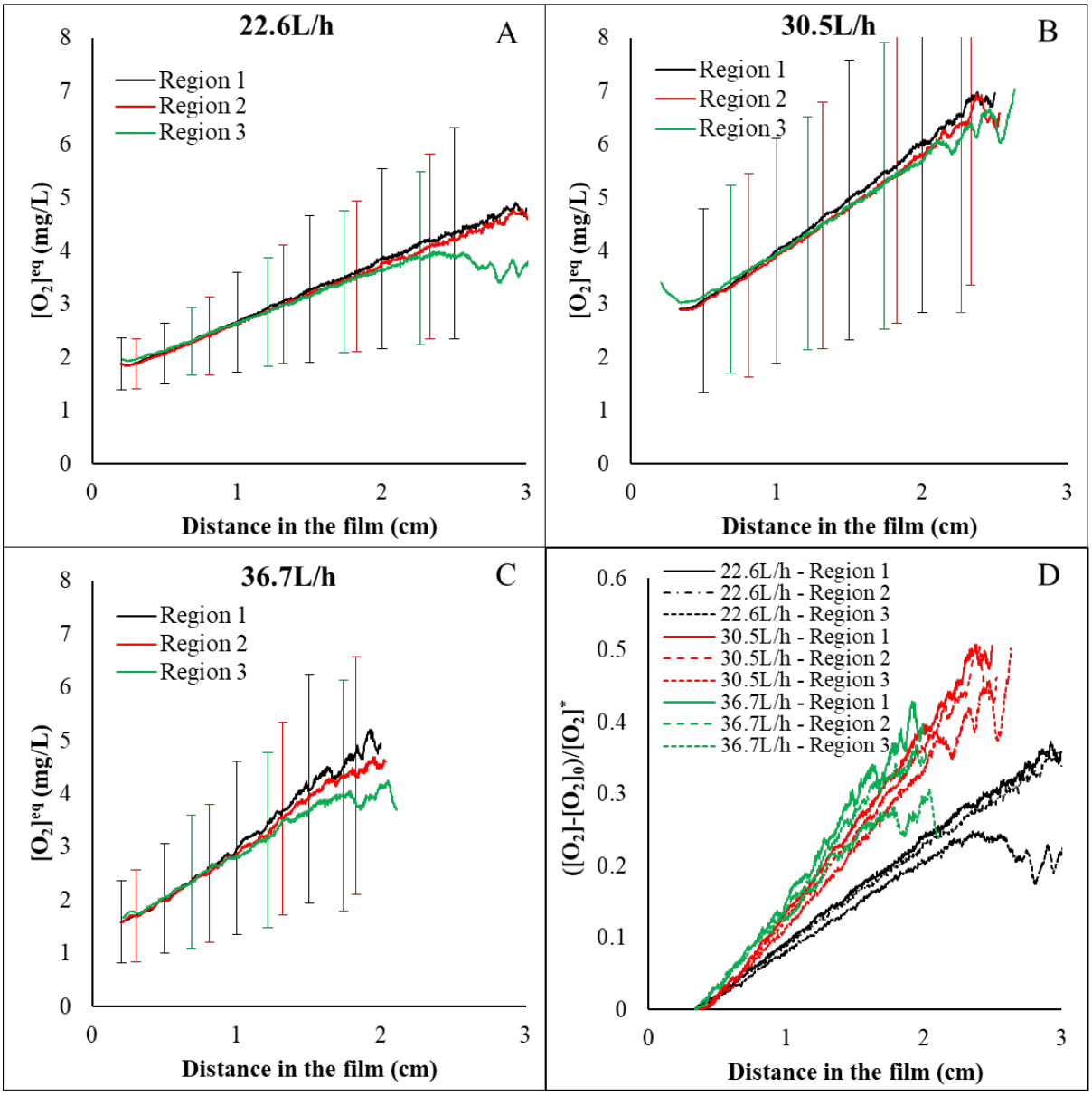


Fig.11: Equivalent dioxygen concentration profile along the liquid film determined by Eq.5 derived from the Beer-Lambert law. Errors bars represent the standard deviation of 6 acquisitions of the spraying of the experimental solution. For clarity they are represented only in some points of the profiles.

As expected, the dioxygen concentration increased in the liquid along the film as shown in Fig.11(A, B, C). Since dioxygen was present in the gas phase and absent in the liquid phase, a strong difference in concentration existed and was favorable to the maximization of the driving force promoting the oxygen mass transfer. For the 22.6 L/h flowrate, the equivalent dioxygen concentration started at around 2 mg/L at the beginning of the optical window (0.3 cm into the film) and reached values around 5 mg/L after only 3 cm in region 1.

For the 22.6 and 36.7 L/h conditions, the first concentration measured at 0.3 cm in the film was around 2

494 mg/L, while it was expected to be 0 since no transfer occurred before the spraying. The experimental
495 solution was probably oxidized by some adsorbed dioxygen present in the tubing between the nozzle and
496 the tank due to air leaks. In any case, as stated earlier, there was no dioxygen in the liquid since reaction
497 occurred in the bulk liquid. By removing the initial concentration of each curve and normalizing with the
498 saturation concentration $[O_2]^*$ it was possible to compare the evolution of equivalent dioxygen
499 concentration in the film due to the transfer of atmospheric $O_2$ for several conditions, as shown in Fig.11D.
500 The curves obtained seemed to show that the transfer was higher for increasing flowrates since the slope of
501 the respective curves were steeper as the flowrate increased. For the 22.6 L/h flowrate, the dioxygen
502 concentration reached around 35% of saturation after 3 cm in region 1, whereas this rate of saturation was
503 reached after only 2 cm with a flowrate of 30.5 L/h. It was also verified for the 36.7 L/h flowrate.
504 Comparison of the equivalent dioxygen profiles for 3 different regions in the film showed that the transfer
505 was not uniform in the liquid film formed during the spraying. For the 22.6 L/h flowrate, the concentration
506 was maximal for the core of the film, represented by region 1 in Fig.3, and it was weaker in observations
507 made closer to the edges of the film. In fact, the slope of the curve for region 1 was higher than that of
508 region 2, indicating a better transfer.
509 The profiles obtained for 30.5 L/h and 36.7 L/h flowrates were quite closer to each other than to the profile
510 for 22.6 L/h flowrate.
511 Although significant errors remained associated with the concentration measurement as shown in Fig.11,
512 the mean values obtained were consistent with the expected theoretical values: a liquid in equilibrium with
513 air at ambient pressure and temperature tends to reach a dissolved concentration of dioxygen of around 8
514 mg/L, as is the case in the literature, where experimental dioxygen absorption in a spray was performed by
515 liquid collection with a similar nozzle and flowrate (Canado et al., 2020). The global measurements
516 performed by liquid collection exhibited a strong increase in concentration between 0 and 3 cm of the spray.
517 After 3 cm, a smooth increase occurred, reaching the saturation value of 8 mg/L. The dioxygen
518 concentration profiles obtained in Canado's study and the present one have been grouped in a common
519 chart in Fig.12 to construct the evolution of the concentration in a whole spray:

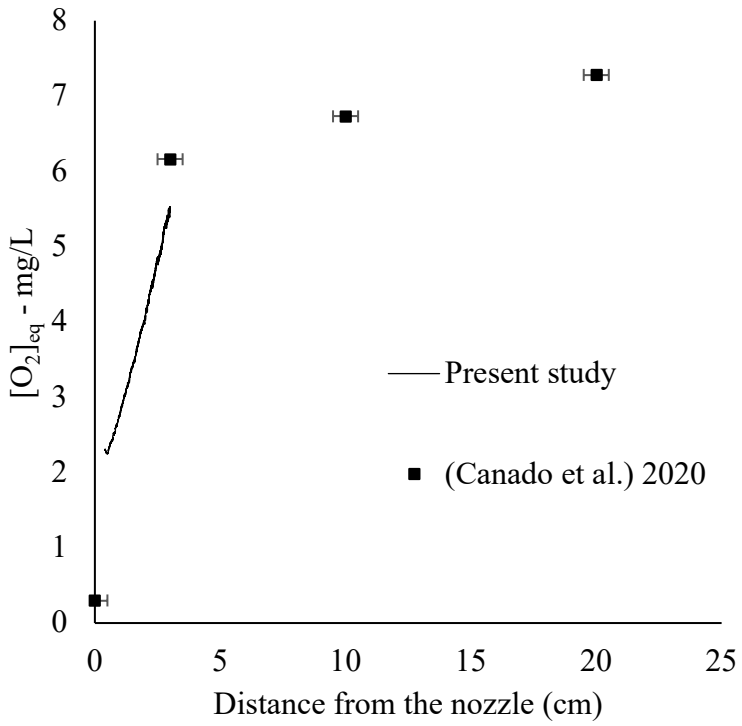


Fig.12: Dioxygen concentration profile obtained by liquid collection (squares) and with the present method (line) for experimental dioxygen absorption in a spray.

As stated in the introduction, liquid collection methods can suffer from end effects leading to an overestimation of the mass transfer occurring between two points of collection. The present method seems to fill the gap between the initial concentration at distance 0 and the concentration of the liquid collected 3 cm downstream, as shown in Fig.12. Both methods highlight a considerable concentration increase by absorption in this region. Thus it is reasonable to attribute the experimental variation measured in this area to mass transfer. This comparison confirms that the mass transfer occurring in the first few centimeters i.e., in the liquid film, was stronger than that occurring once droplets had formed. This transfer enhancement could be explained by a better interfacial area and hydrodynamics conditions of the liquid film region.

### *4.3 Mass transfer analysis*

The liquid side mass transfer coefficient, $k_L$, denotes the strength of the transfer of a solute between two phases. Two approaches for the determination of this coefficient have been proposed. First, local analyses based on the evolution of the concentration pixel by pixel (i.e., $\frac{d[O2]}{dz}$) for different positions in the film

were performed using Eq.9. This provided an accurate description of the evolution of the transfer along the film. Using Eq.10, a global analysis for a considerable section of the film (1.8 cm length) was performed to obtain a value of $\overline{k_L}$ able to represent the whole liquid film. The local analysis was performed for 3 different flowrates and 4 positions, and the mean results are reported in Fig.13 and Table 2.

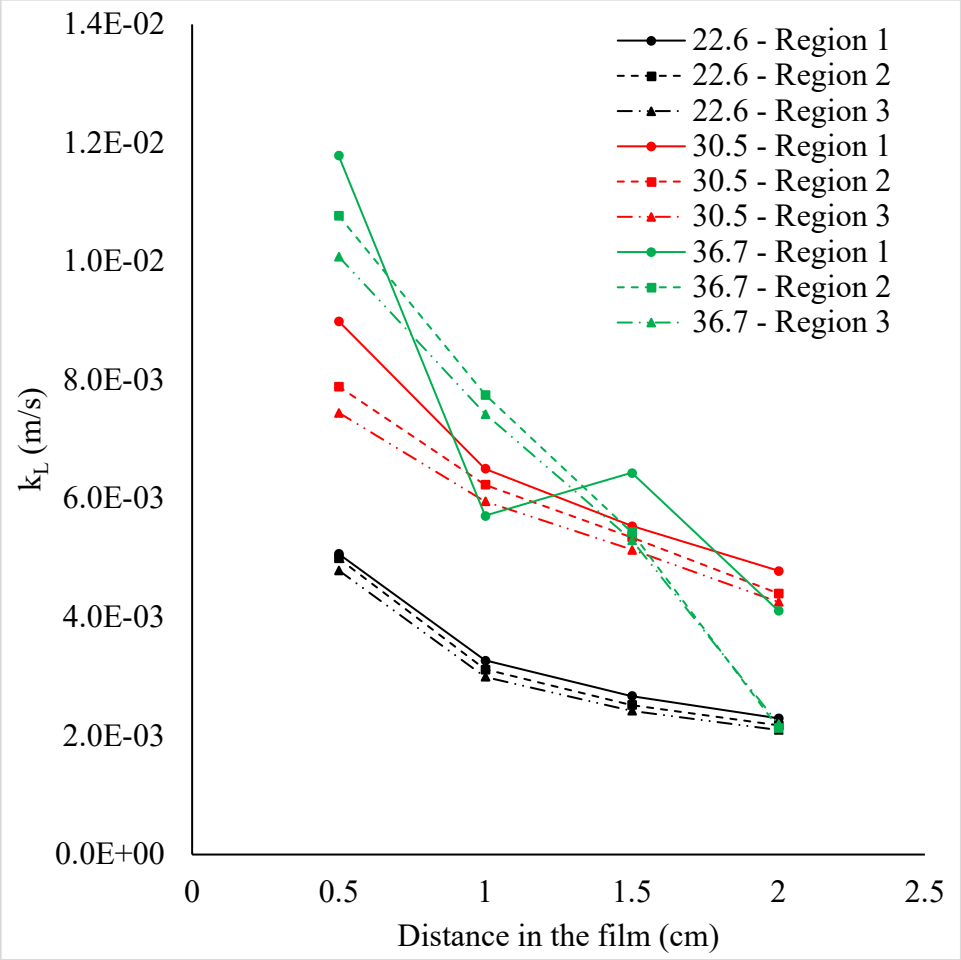


Fig.13: Local liquid side mass transfer coefficient determined with Eq.9 for different flowrates.

Fig.13 reports a common behavior of mass transfer, i.e. the increase of $k_L$ with the velocity of the fluid. For a given cross section of the nozzle, increasing the flowrate leads to an augmentation of the velocity of the fluid. Thus, it seemed logical to see $k_L$ increase with the flowrate. For each flowrate, region 1 exhibited higher values of $k_L$ than regions 2 and 3, confirming a stronger transfer in the core of the liquid film than near the edges of the film.

The local analysis presented in Fig.13 and Table 2 allowed the decrease of mass transfer with distance in the film to be observed. For all the flowrates, high values of the mass transfer coefficient were determined at 0.5 cm in the film, whereas lower values were measured after 2 cm in the liquid film. For instance, at

22.6 L/h, $k_L$ reached 5.1 x $10^{-3}$ m/s at 0.5 cm in the film, but it had half this value at z = 2 cm, with a value of 2.3 x $10^{-3}$ m/s. This behavior was observed for all the regions and all the flowrates tested in the present study. These results might express the deceleration of the liquid along the film since $k_L$ is related to the velocity of the fluid. The liquid exits the nozzle with a velocity of around 12.98 m/s as stated in Table.2, and the velocities of the droplets have been measured at around 8.5 m/s in a previous study (Canado et al., 2020) for a similar nozzle and flowrate, indicating a decrease in velocity of the liquid film from the orifice to the formation of droplets. According to the shape of the orifice, the film spreads with a given geometry and angle, and the friction with air causes instabilities to grow in its core and decrease its velocity, so it seems consistent to attribute the decrease of the $k_L$ with distance to the decrease of the velocity of the liquid along the film.

Note that the results for the 36.7L/h seemed to dramatically decrease with the distance, especially for the 1.5 and 2cm distance, compared to the lower flowrates. It did not seem reasonable to attribute this behavior to a mass transfer phenomenon but rather an uncertainty of measurement. Compared to the 22.6L/h and 30.5L/h flowrate, at 2cm, the dioxygen concentration profile for the 36.7L/h was not linear such as the two other flowrates. The variations on this curve interfere with the calculation of dO2/dz, that allow the calculation of local $k_L$. Thus, the resulting kL can be in contradiction with the ones determined for an almost linear curve as the 22.6L/h and 30.5L/h dioxygen concentration profiles. Also, the optical window of the higher flowrate was defined for 2% error with the Fresnel equation instead of 1% for the lower flowrates in Fig.4.

| **Local analysis** | | | | | | |
|---|---|---|---|---|---|---|
| ***Parameters*** | | | | ***Region 1*** | ***Region 2*** | ***Region 3*** |
| **Q** (L/h) | **U** (m/s) | **z** (cm) | **w** (cm) | **$k_L.10^3$** (m/s) | | |
| 22.6 | 7.99 | 0.5 | 0.84 | 5.1 | 5.0 | 4.8 |
| | | 1 | 1.38 | 3.3 | 3.1 | 3.0 |
| | | 1.5 | 1.71 | 2.7 | 2.5 | 2.4 |
| | | 2 | 1.91 | 2.3 | 2.2 | 2.1 |
| 30.5 | 10.79 | 0.5 | 0.93 | 9.0 | 7.9 | 7.5 |
| | | 1 | 1.56 | 6.5 | 6.2 | 6.0 |
| | | 1.5 | 1.99 | 5.5 | 5.3 | 5.1 |

| | | | | | | |
|---|---|---|---|---|---|---|
| | | 2 | 2.29 | 4.8 | 4.4 | 4.3 |
| 36.7 | 12.98 | 0.5 | 0.89 | 11.8 | 10.8 | 10.1 |
| | | 1 | 1.69 | 5.7 | 7.8 | 7.4 |
| | | 1.5 | 2.12 | 6.4 | 5.4 | 5.3 |
| | | 2 | 2.35 | 4.1 | 2.1 | 2.2 |

Table 2: Values used for the calculation of $k_L$ and the values of $k_L$ determined with Eq.7.

The results of the global analysis presented in Table 3 confirm the increase of $\overline{k_L}$ in the film with the flowrates. The difference of transfer between the 3 regions of study is also confirmed, since the $\overline{k_L}$ values determined for region 1 are higher than those determined for regions 2 and 3. The global analysis provides values of $\overline{k_L}$ able to represent the whole liquid film and that can be used for the determination of correlations for the mass transfer during the formation stage of the droplets by spraying.

| | **Global analysis** | | | | |
|---|---|---|---|---|---|
| **Z** (cm) | **Q** (L/h) | $\bar{w}$ (cm) | | **ΔC** (mg/L) | $\overline{k_L}.10^3$ (m/s) |
| 1.8 | 22.6 | 1.56 | Region 1 | 1.98 | 2.8 |
| | | | Region 2 | 1.91 | 2.7 |
| | | | Region 3 | 1.79 | 2.5 |
| | 30.5 | 1.83 | Region 1 | 3.10 | 5.0 |
| | | | Region 2 | 2.99 | 4.8 |
| | | | Region 3 | 3.02 | 4.8 |
| | 36.7 | 1.84 | Region 1 | 3.44 | 6.6 |
| | | | Region 2 | 2.96 | 5.7 |
| | | | Region 3 | 2.52 | 4.9 |

Table 3: Values used for the calculation of $\overline{k_L}$ and the values of $\overline{k_L}$ determined with Eq.9.

From those global $k_L$ and considering a reaction rate, k, of 1.28 x $10^6$ $L.mol^{-1}.s^{-1}$ as stated in the literature (Yang et al., 2016), the Hatta number was assessed at between 0.23 and 0.54. Hatta values under 0.3 mean that the reaction between the $O_2$ and the dye does not accelerate the rate of transfer of $O_2$ from the air into the liquid. Thus, it is possible to consider that the rate of transfer measured with the present method corresponds to the actual rate of transfer occurring in the liquid film. In other words, the method does not change the regime of transfer occurring in the liquid film.

Moreover, this means that no accumulation of dioxygen occurred in the liquid; it was instantly consumed by the reaction.

No correlations are currently available in the literature for the formation stage of droplets during the

584 spraying. An effort has been made to plot the correlation between the mass transfer occurring in the liquid
585 film, denoted by the Sherwood number, and its hydrodynamics, expressed with the Reynolds number.
586
587 From the three different flowrates tested, a power law has been assessed to link the Sherwood and Reynolds
588 numbers based on the thickness of the liquid as the characteristic scale:
589 $$Sh = 0.0052\ Re^{1.783}$$
590 Although the few conditions investigated here were not enough to perform a complete, rigorous mass
591 transfer analysis, the example of analysis given shows that it is possible to observe an acceptable correlation
592 ($R^2$=0.995) between the mass transfer and the hydrodynamics of the liquid film with the present method.
593 Commonly, such correlations for mass transfer with droplets or bubbles for steady flows propose a
594 Reynolds number with the power 0.5 (Codolo and Bizzo, 2013; Kumar and Hartland, 1999; Tanda et al.,
595 2011). The present correlation revealed a strong effect of the Reynolds number on the mass transfer since
596 the exponent found was equal to 1.783. This behavior has already been shown for mass transfer during the
597 breakup of a cylindrical jet (Srinivasan and Aiken, 1988). This result marked the importance of the flowrate
598 for the mass transfer in the formation stage of droplets compared to systems with settled droplets. The
599 present analysis had to be carefully considered since a small range of flowrates was tested because the
600 nozzle used had a reduced range of operating regime.
601 With this light absorption technique, it should be possible, in the future, to study the liquid film region to
602 propose several correlations between the mass transfer and the operating conditions. In addition with the
603 numerous existing methods for droplets characterization, the present method would allow a full description
604 of the mass transfer occurring in the spray, from the formation stage of the droplets (in the first centimeters)
605 to the cloud of droplets (as far as 1 meter downstream). The methods for liquid film and droplets
606 characterization complement each other to better understand the mass transfer occurring in sprays. Finally,
607 from the mass transfer analysis performed using dioxygen, the transfer for any solute in the liquid film can
608 be predicted with mass transfer theories.

## 5. Conclusions

A light absorption method has been successfully applied to measure the thickness of an atomizing liquid film. By using the dioxygen sensitive dye resazurin, the profile of dioxygen diffusing along this liquid film has been determined.

The liquid film was subject to growing instabilities that, once they reached a considerable amplitude, tore the liquid apart into droplets. The wavy motion induced by those instabilities produced dark folds in the film, leading to local losses of intensity. Despite that, the linearity of the Beer-Lambert law has been proven for different places along the film, allowing the thickness and concentration profile to be determined quantitatively. An example of mass transfer analysis has been presented to show the interest of the method. The latter analysis required concentration measurements that were performed thanks to the present method. This analysis led to the confirmation that the formation stage of the droplets enabled a higher mass transfer than the droplets once they were formed. A local analysis showed a decrease of the transfer along the distance of the film from the nozzle but also from the core of the liquid to the edges. Hatta numbers have been assessed from the mass transfer coefficient obtained and confirm that the present method correctly reports the actual regime of transfer occurring in the liquid film.

In the literature, mass transfer analysis of atomizing liquid film has commonly been global analysis performed by liquid collection and titration. The present method has the advantage of proposing a local analysis of the liquid film and the results are in good agreement with global studies. For the future, an effort must be made to challenge the method with different geometries of liquid film (conical, full conical, etc.), and flow conditions (flowrates/pressure), to propose correlations able to predict the mass transfer during the formation stage of the droplets.

## Acknowledgments

This research is part of to the SOLSTICE project supported by the French state within the framework of "Programme d'Investissements d'Avenir"

## References


Ashgriz, N. (Ed.), 2011. Handbook of Atomization and Sprays. Springer US, Boston, MA. https://doi.org/10.1007/978-1-4419-7264-4

Brübach, J., Patt, A., Dreizler, A., 2006. Spray thermometry using thermographic phosphors. Appl. Phys. B 83, 499–502. https://doi.org/10.1007/s00340-006-2244-8

Buijs, K., Maurice, M.J., 1969. Some considerations on apparent deviations from lambert-beer's law. Anal. Chim. Acta 47, 469–474. https://doi.org/10.1016/S0003-2670(01)95647-8

Canado, A., Tournois, M., Pages, M., Roustan, M., Remus-Borel, W., Dietrich, N., Violleau, F., Hébrard, G., 2020. Sudden Decrease of the Dissolved Ozone Concentration in Sprays: A Mass Transfer Phenomenon? Ind. Eng. Chem. Res. 59, 14914–14924. https://doi.org/10.1021/acs.iecr.0c03216

Codolo, M.C., Bizzo, W.A., 2013. Experimental study of the SO2 removal efficiency and volumetric mass transfer coefficients in a pilot-scale multi-nozzle spray tower. Int. J. Heat Mass Transf. 66, 80–89. https://doi.org/10.1016/j.ijheatmasstransfer.2013.07.011

Dietrich, N., Hebrard, G., 2018. Visualisation of gas-liquid mass transfer around a rising bubble in a quiescent liquid using an oxygen sensitive dye. Heat Mass Transf. 54, 2163–2171. https://doi.org/10.1007/s00231-018-2297-3

Dietrich, N., Loubière, K., Jimenez, M., Hébrard, G., Gourdon, C., 2013. A new direct technique for visualizing and measuring gas–liquid mass transfer around bubbles moving in a straight millimetric square channel. Chem. Eng. Sci. 100, 172–182. https://doi.org/10.1016/j.ces.2013.03.041

Dietrich, N., Wongwailikhit, K., Mei, M., Xu, F., Felis, F., Kherbeche, A., Hébrard, G., Loubière, K., 2019. Using the "red Bottle" Experiment for the Visualization and the Fast Characterization of Gas-Liquid Mass Transfer. J. Chem. Educ. 96, 979–984. https://doi.org/10.1021/acs.jchemed.8b00898

Dumouchel, C., 2008. On the experimental investigation on primary atomization of liquid streams. Exp. Fluids 45, 371–422. https://doi.org/10.1007/s00348-008-0526-0

Fansler, T.D., Parrish, S.E., 2015. Spray measurement technology: A review. Meas. Sci. Technol. 26. https://doi.org/10.1088/0957-0233/26/1/012002

Hariz, R., del Rio Sanz, J.I., Mercier, C., Valentin, R., Dietrich, N., Mouloungui, Z., Hébrard, G., 2017. Absorption of toluene by vegetable oil–water emulsion in scrubbing tower: Experiments and modeling. Chem. Eng. Sci. 157, 264–271. https://doi.org/10.1016/j.ces.2016.06.008

Hegely, L., Roesler, J., Alix, P., Rouzineau, D., Meyer, M., 2017. Absorption methods for the determination of mass transfer parameters of packing internals: A literature review. AIChE J. 63, 3246–3275. https://doi.org/10.1002/aic.15737

Kherbeche, A., Mei, M., Thoraval, M.-J., Hébrard, G., Dietrich, N., 2020. Hydrodynamics and gas-liquid mass transfer around a confined sliding bubble. Chem. Eng. J. 386, 121461. https://doi.org/10.1016/j.cej.2019.04.041

Kherbeche, A., Milnes, J., Jimenez, M., Dietrich, N., Hébrard, G., Lekhlif, B., 2013. Multi-scale analysis of the influence of physicochemical parameters on the hydrodynamic and gas–liquid mass transfer in gas/liquid/solid reactors. Chem. Eng. Sci. 100, 515–528. https://doi.org/10.1016/j.ces.2013.06.025

Kim, S., Khil, T., Kim, D., Yoon, Y., 2009. Effect of geometric parameters on the liquid film thickness and air core formation in a swirl injector. Meas. Sci. Technol. 20, 015403. https://doi.org/10.1088/0957-0233/20/1/015403

Koralek, J.D., Kim, J.B., Brůža, P., Curry, C.B., Chen, Z., Bechtel, H.A., Cordones, A.A., Sperling, P., Toleikis, S., Kern, J.F., Moeller, S.P., Glenzer, S.H., DePonte, D.P., 2018. Generation and characterization of ultrathin free-flowing liquid sheets. Nat. Commun. 9, 1353. https://doi.org/10.1038/s41467-018-03696-w

Kumar, A., Hartland, S., 1999. Correlations for Prediction of Mass Transfer Coefficients in Single Drop Systems and Liquid–Liquid Extraction Columns. Chem. Eng. Res. Des. 77, 372–384. https://doi.org/10.1205/026387699526359

Lebrun, G., Xu, F., Le Men, C., Hébrard, G., Dietrich, N., 2021. Gas–Liquid Mass Transfer around a Rising Bubble: Combined Effect of Rheology and Surfactant. Fluids 6, 84. https://doi.org/10.3390/fluids6020084

Lefebvre, A., Mcdonell, V., 2017. Atomization and Sprays, Second Edition., Boca Raton: CRC Press.

https://doi.org/10.1016/0009-2509(90)87140-N

Lefebvre, A.H., 1989. Properties of Sprays. Part. Part. Syst. Charact. 6, 176–186. https://doi.org/10.1002/ppsc.19890060129

Lemoine, F., Castanet, G., 2013. Temperature and chemical composition of droplets by optical measurement techniques: a state-of-the-art review. Exp. Fluids 54, 1572. https://doi.org/10.1007/s00348-013-1572-9

Lépinasse, E., Marion, M., Guella, S., Alexandrova, S., Saboni, A., 2012. Absorption et désorption du dioxyde de souffre par des gouttes d'eau de fort diamètre en chute. Sulfur dioxide absorption and desorption by large free falling water droplets. Rev. des Sci. l'eau 18, 5. https://doi.org/10.7202/705547ar

Lin, W.-C., Rice, P.A., Cheng, Y.-S., Barduhn, A.J., 1977. Vacuum stripping of refrigerants in water sprays. AIChE J. 23, 409–415. https://doi.org/10.1002/aic.690230402

Maeda, H., MATSU-URA, S., SENBA, T., YAMASAKI, S., TAKAI, H., YAMAUCHI, Y., OHMORI, H., 2000. Resorufin as an Electron Acceptor in Glucose Oxidase-Catalyzed Oxidation of Glucose. Chem. Pharm. Bull. (Tokyo). 48, 897–902. https://doi.org/10.1248/cpb.48.897

Mei, M., Hébrard, G., Dietrich, N., Loubière, K., 2020. Gas-liquid mass transfer around Taylor bubbles flowing in a long, in-plane, spiral-shaped milli-reactor. Chem. Eng. Sci. 222, 115717. https://doi.org/10.1016/j.ces.2020.115717

Mendez, M.A., Németh, L., Buchlin, J.M., 2016. Measurement of Liquid Film Thickness via Light Absorption and Laser Tomography. EPJ Web Conf. 114. https://doi.org/10.1051/epjconf/201611402072

Reitz, R.D., 1982. Mechanism of atomization of a liquid jet. Phys. Fluids 25, 1730. https://doi.org/10.1063/1.863650

Rizk, N.K., Lefebvre, A.H., 1980. The Influence of Liquid Film Thickness on Airblast Atomization. J. Eng. Power 102, 706–710. https://doi.org/10.1115/1.3230329

Shao, T., Feng, X., Wang, W., Jin, Y., Cheng, Y., 2012. Visualization of coupled mass transfer and reaction

between gas and a droplet using a novel reactive-PLIF technique. Chem. Eng. J. 200–202, 549–558. https://doi.org/10.1016/j.cej.2012.06.113

Simpson, S.G., Lynn, S., 1977. Vacuum-spray stripping of sparingly soluble gases from aqueous solutions: Part I. Mass transfer from streams issuing from hydraulic nozzles. AIChE J. 23, 666–673. https://doi.org/10.1002/aic.690230507

Srinivasan, V., Aiken, R.C., 1988. Mass transfer to droplets formed by the controlled breakup of a cylindrical jet—physical absorption. Chem. Eng. Sci. 43, 3141–3150. https://doi.org/10.1016/0009-2509(88)85123-6

Strizhak, P., Volkov, R., Moussa, O., Tarlet, D., Bellettre, J., 2020. Measuring temperature of emulsion and immiscible two-component drops until micro-explosion using two-color LIF. Int. J. Heat Mass Transf. 163, 120505. https://doi.org/10.1016/j.ijheatmasstransfer.2020.120505

Suyari, M., Lefebvre, A.H., 1986. Film thickness measurements in a simplex swirl atomizer. J. Propuls. Power 2, 528–533. https://doi.org/10.2514/3.22937

Swinehart, D.F., 1962. The Beer-Lambert Law. J. Chem. Educ. 39, 333. https://doi.org/10.1021/ed039p333

Tanda, T., Shirai, K., Matsumura, Y., Kitahara, H., 2011. New Correlation for Mass Transfer Characteristics of Spray Column. Ind. Eng. Chem. Res. 50, 13554–13560. https://doi.org/10.1021/ie200989k

Tatin, R., Moura, L., Dietrich, N., Baig, S., Hébrard, G., 2015. Physical absorption of volatile organic compounds by spraying emulsion in a spray tower: Experiments and modelling. Chem. Eng. Res. Des. 104, 409–415. https://doi.org/10.1016/j.cherd.2015.08.030

Träger, F., 2012. Springer Handbook of Lasers and Optics, Springer Handbooks. Springer Berlin Heidelberg.

Volkov, R.S., Strizhak, P.A., 2018. Using Planar Laser Induced Fluorescence to explore the mechanism of the explosive disintegration of water emulsion droplets exposed to intense heating. Int. J. Therm. Sci. 127, 126–141. https://doi.org/10.1016/j.ijthermalsci.2018.01.027

Weber, M.J., 2018. Handbook of Optical Materials, 1st Editio. ed. CRC Press. https://doi.org/10.1201/9781315219615

Wegener, M., Paschedag, A.R., Kraume, M., 2009. Mass transfer enhancement through Marangoni

instabilities during single drop formation. Int. J. Heat Mass Transf. 52, 2673–2677. https://doi.org/10.1016/j.ijheatmasstransfer.2009.01.005

Xu, J.H., Tan, J., Li, S.W., Luo, G.S., 2008. Enhancement of mass transfer performance of liquid–liquid system by droplet flow in microchannels. Chem. Eng. J. 141, 242–249. https://doi.org/10.1016/j.cej.2007.12.030

Xue, T., Zhang, S., 2018. Investigation on heat transfer characteristics of falling liquid film by planar laser-induced fluorescence. Int. J. Heat Mass Transf. 126, 715–724. https://doi.org/10.1016/j.ijheatmasstransfer.2018.05.039

Yang, L., Dietrich, N., Hébrard, G., Loubière, K., Gourdon, C., 2017. Optical methods to investigate the enhancement factor of an oxygen-sensitive colorimetric reaction using microreactors. AIChE J. 63, 2272–2284. https://doi.org/10.1002/aic.15547

Yang, L., Dietrich, N., Loubière, K., Gourdon, C., Hébrard, G., 2016. Visualization and characterization of gas–liquid mass transfer around a Taylor bubble right after the formation stage in microreactors. Chem. Eng. Sci. 143, 364–368. https://doi.org/10.1016/j.ces.2016.01.013

Yeh, N.K., Rochelle, G.T., 2003. Liquid-phase mass transfer in spray contactors. AIChE J. 49, 2363–2373. https://doi.org/10.1002/aic.690490912

Zhang, J.T., Wang, B.X., Peng, X.F., 2000. Falling liquid film thickness measurement by an optical-electronic method. Rev. Sci. Instrum. 71, 1883–1886. https://doi.org/10.1063/1.1150557